Quantifying the Impact of Spatial Resolution on Endmember Extraction from Hyperspectral Imagery

J. Plaza, P. Martínez, A. Plaza, and R. Pérez[a]

[a] Neural Networks and Signal Processing Group, Computer Science Department
University of Extremadura, Avda. de la Universidad s/n, E-10071 Cáceres, Spain
email: {jplaza, pablomar, aplaza, rosapere}@unex.es

ABSTRACT

Spectral mixing is a phenomenon that occurs naturally and frequently in real-world scenarios. This phenomenon, which has traditionally been modeled by using both linear and nonlinear techniques, has been reported to significantly influence the task of estimating fractional covers from mixed pixels. Over the past years, several algorithms have been developed for spectral unmixing of hyperspectral data. Many of these algorithms rely on the identification of pure spectral signatures, called endmembers in hyperspectral analysis terminology, which are usually associated to ground constituents in the scene. Due to a lack of quantitative approaches to substantiate new endmember extraction algorithms, available methods have not been rigorously compared using a unified scheme. As a result, very few efforts exist in the literature related to the application of such algorithms to hyperspectral scenes with different spatial resolutions. Our major goal in this paper is to substantiate the impact of spatial resolution of observed pixels on endmember determination techniques. This is achieved by evaluating the accuracy of endmember extraction and subsequent fractional cover estimation using scenes with different pixel sizes. In particular, we demonstrate in this work that the suitability of using spectral mixture models based on endmember signatures is strongly dependent on the considered pixel size. Another goal of the present paper is the generation of a collection of test images that can be used by the scientific community to validate endmember selection methods in light of different spatial resolutions. In order to satisfy the above objectives, we use real hyperspectral data acquired by the DRL ROSIS imaging spectrometer at two different altitudes (3600 and 1940 meters), over a Dehesa area in Extremadura, SW Spain. Dehesa is an agroforestry and pasture agroecosystem that is mainly formed by soils, pasture and cork-oak trees (*Quercus ilex* and *Quercus suber*). Three standard algorithms, i.e. Boardman's Pixel Purity Index (PPI), Winter's N-FINDR, and our own approach, Automated Morphological Endmember Extraction (AMEE), are used in this work to carry out a quantitative and comparative analysis of the influence of algorithm performance in the presence of different spatial resolutions.

Keywords: Spectral mixture analysis, Spatial resolution, Endmember extraction.

1 INTRODUCTION

Spatially referenced and consistently calibrated satellite/airborne image data are very useful in many different applications, including target detection and environmental modeling. The regular spacing of the image data is compatible with the grid formulation of several spatially explicit models [1]. These models assume that physical quantities are averaged over similar shaped areas. In the case of hyperspectral imaging systems [2], the instrument averages radiance and/or reflectance from an area on the surface that corresponds with the sensor field of view and, as a result, any parameter/property derived from that radiance/reflectance is some average of the real values over that area. Although geometric sensor and platform modeling techniques have been shown to yield high quality geometric registrations in many situations, most of these approaches introduce random pixel replacement and/or averaging with respect to neighboring pixels [3], thus producing spatially referenced data at the cost of integrating the original signal, collected at the sensor, with other different spectral signal sources. A major question arises at this point: how well does an estimate, derived from that radiance/reflectance, correspond to the spatial average produced by the models?. This question is particularly relevant when very accurate spectral modeling is required. In this regard, the main purpose of this work is to examine the errors that arise when estimating spatially averaged geophysical parameters from remotely sensed hyperspectral data, where spectral measurements originally collected by the sensor may have been modified by virtue of geo-registration-based pre-processing. In particular, we focus on the problem of estimating surface fractional covers by using spectral mixture models, where it has been found in

Presented at the 3rd EARSeL Workshop on Imaging Spectroscopy, Herrsching, May 13-16 2003

previous work that significant errors can be encountered if the estimated abundance fractions are not properly assigned to the correspondent pixel areas given by the sampling interval of the imaging system [4].

A commonly accepted approach in the literature devoted to spectral mixture analysis is linear spectral unmixing [5]. Such a method applies a linear mixture model to estimate the abundance fractions of spectral signatures within mixed pixels. These pixels involve a mixture of more than one distinct substance, and exist for one of two reasons. First, if the spatial resolution of the sensor is not high enough to separate different materials, these can jointly occupy a single pixel, and the resulting spectral measurement is a composite of the individual spectra. The concept of mixed pixel directly relates to the idea of spatially averaged variables mentioned above. Secondly, mixed pixels may also result when distinct materials are combined into homogeneous mixtures. The linear mixture model can be mathematically defined as follows.

Let $\boldsymbol{h}(x, y)$ be the hyperspectral signature collected by the sensor at the pixel with spatial coordinates (x, y). This signature can be considered an N-dimensional ($N-D$) vector, where N is the number of spectral bands. This vector can be modeled as a linear combination of pure component spectra, called endmember vectors $\boldsymbol{e}_i$, $i = 1,...,E$, by using the following expression

$$\boldsymbol{h}(x, y) = \sum_{i=1}^{E} \Phi_i(x, y) \cdot \boldsymbol{e}_i \,, \tag{1}$$

where $\Phi_i(x, y)$ is a scalar value representing the fractional coverage of endmember $\boldsymbol{e}_i$ at pixel $\boldsymbol{h}(x, y)$. In the above expression, the multivariate signal is unmixed to provide estimates of the fractional coverage of different surface materials within the sensor field of view [6]. The success of this method depends on a number of factors, such as good spectral separation of the endmember spectra with respect to image noise, and high signal-to-noise ratio (SNR). Recent studies [7] have shown that, even if these sources of error can be ignored, there may still be a considerable retrieval error that can be attributed directly to the uneven spatial sampling of the radiance/reflectance within the field of view. As a result, two key tasks in linear spectral mixture analysis are i) to find an appropriate suite of pure spectral signatures (endmembers), which can be used to model at-sensor pixel spectra through a linear combination of endmember signatures, and ii) to substantiate the impact of spatial resolution on the endmember identification procedures.

With an increasing number of automated endmember extraction methods readily available, the need for standardized strategies to evaluate the impact of spatial averaging and geo-registration effects, introduced by spatially explicit models, on the quality of selected endmembers, has been identified as a desired goal by the remote sensing community. In order to achieve the above goal, we use ROSIS data at different altitudes, acquired as part of the 2001 DLR DAIS/ROSIS HySens campaign [8], over a so-called 'Dehesa' area in Cáceres, SW Spain [9], to carry out a comparative analysis of available methods. Another major goal of this work is the generation of a database of test images that can be used to substantiate performance of endmember extraction and hyperspectral unmixing algorithms with regards to differing spatial resolutions. These sets of images are expected to provide the remote sensing community with standardized benchmark data to validate new and available hyperspectral analysis methodologies. The rest of the paper is organized as follows. Section 2 presents an overview of the three endmember extraction algorithms that will be compared in this work. Section 3 describes the hyperspectral image data, along with ground-truth and calibration details. In Section 4, a comparative performance analysis, in terms of spatial resolution, is presented and discussed for the algorithms described in section 2. Section 5 concludes with some remarks and future lines of interest.

2 ENDMEMBER EXTRACTION METHODS

The three endmember extraction algorithms described in this section represent substantially different design choices. Boardman's Pixel Purity Index (PPI) [10] and Winter's N-FINDR [11] might be characterized as instances of the classic approach to endmember selection, based on the search for spectral convexities in $N-D$ space. While PPI is partially automated, N-FINDR is fully automated. Contrary to the methods above, which rely on spectral properties of the data alone, Plaza et al.'s Automated Morphological Endmember Extraction (AMEE) [12] uses a morphological approach where spatial and spectral information are equally employed to derive image endmembers.

2.1 Pixel Purity Index (PPI)

The PPI algorithm is characteristic in its supervised nature; it consists of the following steps: First, a "noise-whitening" and dimensionality reduction step is performed by using the MNF transform [10]. Then, a pixel purity score is calculated for each point in the image cube by randomly generating L lines in the $N-D$ space comprising

the MNF-transformed data. All the points in that space are projected onto the lines, and the ones falling at the extremes of each line are counted. After many repeated projections to different random lines, those pixels that count above a certain cutoff threshold C are declared "pure". These potential endmember spectra are loaded into an interactive $N-D$ visualization tool and rotated in real time until a desired number of endmembers, E, are visually identified as extreme pixels in the data cloud.

2.2 N-FINDR

The N-FINDR method finds the set of pixels which define the simplex with the maximum volume, potentially inscribed within the dataset. First, a dimensionality reduction of the original image is accomplished by using the MNF transform. Next, randomly selected pixels qualify as endmembers, and a trial volume is calculated as follows. Let $\mathbf{E}$ be defined as

$$\mathbf{E} = \begin{bmatrix} 1 & 1 & \dots & 1 \\ \boldsymbol{e}_1 & \boldsymbol{e}_2 & \dots & \boldsymbol{e}_{\mathrm{E}} \end{bmatrix}, \tag{2}$$

where $\boldsymbol{e}_{\mathrm{i}}$ are endmember column vectors and E is the total number of endmembers. The volume of the simplex formed by the endmembers is proportional to the determinant of $\mathbf{E}$

$$\mathrm{V}(\mathbf{E}) = \frac{1}{(\mathrm{E}-1)!}\,\mathrm{abs}\left(\left|\mathbf{E}\right|\right). \tag{3}$$

In order to refine the initial volume estimate, a trial volume is calculated for every pixel in each endmember position by replacing that endmember and recalculating the volume. If the replacement results in a volume increase, the pixel replaces the endmember. This procedure, which does not require any input parameters, is repeated until there are no replacements of endmembers left [11].

2.3 Automated Morphological Endmember Extraction (AMEE)

The input to the AMEE method is the full image data cube, with no previous dimensionality reduction. The method is based on two parameters: a minimum $\mathrm{S}_{\min}$ and a maximum $\mathrm{S}_{\max}$ spatial kernel size. First, a minimum kernel $\mathrm{K} = \mathrm{S}_{\min}$ is considered. This element is moved through all the pixels of the image, defining a spatial context around each hyperspectral pixel $\boldsymbol{h}(\mathrm{x},\mathrm{y})$. The spectrally purest ($\boldsymbol{p}$) and the spectrally most highly mixed ($\boldsymbol{m}$) spectral signatures are respectively obtained at the neighborhood of $\boldsymbol{h}(\mathrm{x},\mathrm{y})$ defined by K using the following extended morphological operations [12].

$$\boldsymbol{p} = \arg\_\mathrm{Max}_{(\mathrm{s,t})\in\mathrm{K}} \left\{ \sum_{\mathrm{s}} \sum_{\mathrm{t}} \mathrm{dist}\left(\boldsymbol{h}(\mathrm{x},\mathrm{y}), \boldsymbol{h}(\mathrm{x}-\mathrm{s},\mathrm{y}-\mathrm{t})\right) \right\}, \qquad \forall\,(\mathrm{s},\mathrm{t}) \in \mathrm{K}, \tag{4}$$

$$\boldsymbol{m} = \arg\_\mathrm{Min}_{(\mathrm{s,t})\in\mathrm{K}} \left\{ \sum_{\mathrm{s}} \sum_{\mathrm{t}} \mathrm{dist}\left(\boldsymbol{h}(\mathrm{x},\mathrm{y}), \boldsymbol{h}(\mathrm{x}+\mathrm{s},\mathrm{y}+\mathrm{t})\right) \right\}, \qquad \forall\,(\mathrm{s},\mathrm{t}) \in \mathrm{K}, \tag{5}$$

where dist is the spectral angle distance (SAD) [2]. A morphological eccentricity index (MEI) [13] is then obtained by calculating the SAD distance between the two signatures above. This operation is repeated for all the pixels in the scene, using kernels of progressively increased size, and the resulting scores are used to evaluate each pixel in both spatial and spectral terms. The algorithm performs as many iterations as needed until $\mathrm{K} = \mathrm{S}_{\max}$. The associated MEI value of selected pixels at subsequent iterations is updated by means of newly obtained values, as a larger spatial context is considered, until a final MEI image is generated. Endmember selection is performed by a fully automated approach consisting of two steps: 1) autonomous segmentation of the MEI image, and 2) spatial/spectral growing of resulting regions [14].

3 HYPERSPECTRAL IMAGE DATA

The images used in this study were acquired by the DLR ROSIS imaging spectrometer at two different altitudes (1940 and 3600 meters, respectively) on June 21, 2001. Data were collected over a Dehesa area near the town of Cáceres, SW Spain. Dehesa semi-arid ecosystems are mainly formed by cork-oak trees (*Quercus ilex* and *Quercus suber*), soils and pasture. In the southern parts of the Iberian Peninsula, Dehesa areas are traditionally used for a combination of livestock, forest and agriculture activity. Around 12-18% of the area is harvested on a yearly basis

[9]. The crops are used for animal feed or for cash cropping, depending on the rainfall of the area. In such environments, accurate determination of the fractional abundance of materials allows for a better monitoring of natural resources. Each ROSIS overflight included a pass over a Dehesa area called "Finca Cuartillo", as well as the northern campus of University of Extremadura and the "Guadiloba" reservoir (the full flightline is shown in Fig. 1). Collected radiance values were normalized to reflectance using portable field reflectance measurements made on a parking lot adjacent to the University campus. The availability of low-altitude (high-spatial-resolution) and high-altitude (low-resolution) ROSIS data, provides an unprecedented opportunity to compare the radiometric quality, the ability to detect endmembers, and the effectiveness of spectral unmixing techniques in the task of estimating fractional abundances of surface materials. Also, in this study it was possible to remove the uncertainty associated with differing sensor signal-to-noise ratios (SNR's) because the same ROSIS sensor was used to acquire both high-resolution and low-resolution imagery.

Figure 1. Full DAIS/ROSIS flightline over a Dehesa area called "Finca Cuartillo", in Cáceres, SW Spain.

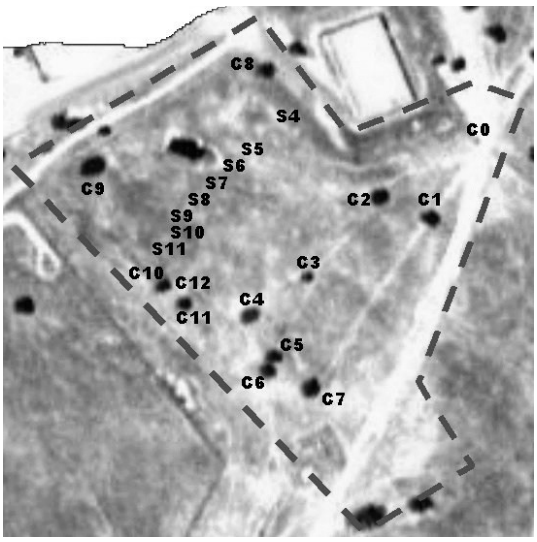

Figure 2. Target study area with labeled objects: cork-oak trees (C0..C11) and soil areas: (S4..S12).

Fig. 2 shows a picture of the selected test site for experiments. Partial ground-truth data were collected at this site using a portable ASD FieldSpec Pro spectro-radiometer and GPS equipment. Field spectral measurements were

used to characterize a series of target objects, including 12 cork-oak trees (labeled as C0...C11) and 9 soil areas (labeled as S4…S12). In the case of cork-oak trees, ground spectral data were acquired at the top of tree crowns, as depicted in Fig. 3. In addition, high-precision GPS data were used to determine the exact spatial localization of the objects. Several control points in a perimeter area surrounding each target object were localized spatially in order to characterize both the area and the edges of each object. Due to observed slight variations between ground-truth GPS data and available image geo-registration, a new approach for accurately matching images at different altitudes was developed. This strategy will be used in experiments in order to carry out a pixel-by-pixel comparison of fractional abundance estimation accuracy by several spectral mixture analysis techniques based on endmember modeling. Before addressing the proposed simple registration technique, which was used to generate the data sets used in experiments, we emphasize that it relies on a pattern recognition-based approach. This type of approach is especially useful when no other geo-registration data is available, or when existing reference information is not accurate enough. The method relies heavily on the rich spectral information provided by hyperspectral imaging systems, and consists of the following steps.

1. A standard spectral matching method was first applied to the two different altitude images in order to identify a target object clearly distinct from the background. In this work, we have applied the spectral angle mapper (SAM) method [2] to identify a cork-oak tree target, which is clearly discernible in the high/low-resolution subscenes. A reference spectral signature, interactively derived from the high-resolution scene, was used to carry out the spectral matching process.
2. Next, the target was separated from background in both the low-altitude and high-altitude subscenes by using the output provided by SAM in combination with a simple adaptative threshold-based procedure.
3. Once the corresponding target object was accurately identified in the two subscenes, the centroid of the object was used as the origin of a new coordinate system. Assuming that each low-resolution image pixel corresponds to four high-resolution image pixels, due to the existing 2:1 ratio in the pixel area for different altitude ROSIS imagery, a sample regular area surrounding the object was defined. This area was used to derive two subscenes covering the same spatial location.
4. As a final step, available ground-truth GPS coordinates were used to validate the accuracy of the proposed registration approach using as control points both the centroid of the object and several pixels in the target edge.

Using the above procedure, we have generated two sets of corresponding high-resolution/low-resolution hyperspectral image pairs that will be used in this study. These images will be designed from now on as high-resolution scene centered at C4 (HRC4, with size of 82x82 pixels), low-resolution scene centered at C4 (LRC4, 41x41 pixels), high-resolution scene centered at C3 (HRC3, 34x34 pixels) and low-resolution scene centered at C3 (LRC3, 17x17 pixels). Fig. 4 shows the two sets of high-resolution/low-resolution image pairs (the spectral band collected at 535 nm wavelength by the ROSIS imaging spectrometer has been considered for visualization purposes). By means of the proposed pattern recognition-based registration technique, HRC3 and LRC3 were derived using the centroid of C3 as a reference, while HRC4 and LRC4 were generated from the centroid of C4.

Figure 3. Ground-truth data collection at the top of C3 tree crown by using an ASD FieldSpec Pro spectroradiometer.

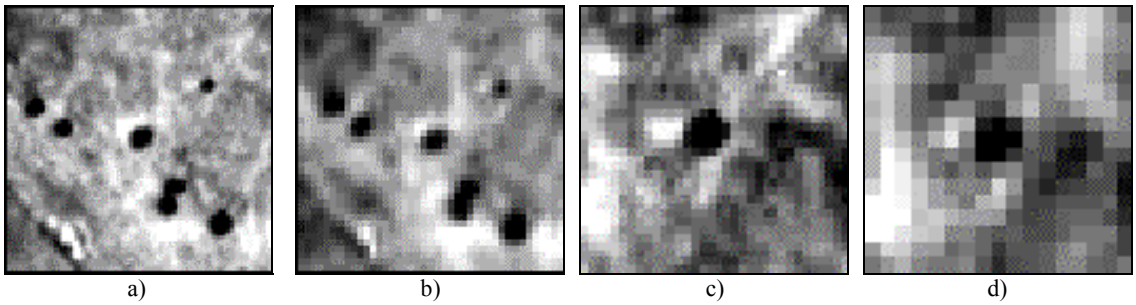

a) b) c) d)

Figure 4. High-resolution/low-resolution hyperspectral image pairs. a) HRC4. b) LRC4. c) HRC3. d) LRC3.

4 COMPARATIVE PERFORMANCE ANALYSIS

This section describes a series of experiments which use hyperspectral subscenes at different spatial resolutions to conduct a comprehensive comparison among standard endmember extraction algorithms [15]. The results shown in this section have been generated using H-COMP [16], a custom designed tool for quantitative and comparative analysis of endmember extraction and hyperspectral unmixing algorithms. A general assumption in the high-resolution imagery can be compared, using a pixel-by-pixel basis, to low-resolution data, since the data is accurately geo-referenced and consistently calibrated (see section 3). Table 1 summarizes the comparative experiments carried out in this work. These experiments will focus on analyzing, with very accurate precision, the impact of the two available spatial resolutions on endmember extraction approaches for spectral mixture analysis of hyperspectral data.

Table 1. Summary of experiments.

Experiment	Datasets used	Objective
1	HRC3, LRC3	To compare algorithm performance in the task of extracting spectral endmembers from hyperspectral data at different spatial resolutions.
2	HRC4, LRC4	To compare estimated fractional abundances obtained by using endmembers derived from hyperspectral data at different spatial resolutions.

4.1 Experiment 1

In order to perform this experiment, we have selected several ground spectral measurements on the test site to be used as ground-truth references in the comparison. These signatures, acquired with a FieldSpec Pro ground spectro-radiometer (see section 3), correspond to different materials that have been identified in the site. We have focused our study on a particular target material, i.e. a cork-oak tree, labeled as C3 in Fig. 2.

Three well-known algorithms for endmember extraction are compared in this section: PPI, N-FINDR and AMEE. As described in section 2, PPI requires close human supervision during the process of determining the endmembers, while N-FINDR and AMEE are fully automated. Prior to a full examination and discussion of results, it is important to outline parameter values used for PPI and AMEE algorithms, bearing in mind that the N-FINDR method does not require any input parameters. In the PPI method, the value of the cutoff threshold parameter C was set to the mean of PPI scores obtained after $L = 10^4$ iterations, so that only pixels with a PPI score above the average were selected as endmember candidates. Pixels were then grouped into smaller subsets based on their clustering in the $N-D$ space. Finally, resulting groups of extreme pixels were linked to the original image, and the mean spectrum of each group was used as a candidate endmember for unmixing. A previous study of AMEE performance revealed that satisfactory results in most situations can be found by setting S_{min} and S_{max} parameters to 3x3 pixels and 15x15 pixels respectively [12]. For illustrative purposes, the cork-oak endmember spectra derived by PPI, N-FINDR and AMEE methods from HRC3 and LRC3 are shown in Fig. 5(a) and Fig. 5(b), respectively. Extracted endmembers have the same reflectance units as the input data, since each endmember is actually the spectum (or an average) of real image pixels. For illustrative purposes, the ground-truth spectrum, collected at the

top of C3 (see Fig. 3), is also plotted in both graphs. This reference signature is expressed in units of scaled reflectance.

It can be noted in Fig. 5(a) that, although there are differences in the scales, spectral shape is mostly preserved in the high-spatial resolution data, being the spectral endmembers derived by N-FINDR and AMEE highly similar, in spectral terms, to the ground-truth cork-oak tree spectrum. In order to determine the best matching endmember for the reference signature, the spectral angle distance between each extracted endmember and the reference is calculated. We have selected the spectral angle distance for the comparison due to existing scale and illumination variations between reference and extracted endmembers. In the case of low-spatial resolution data, as seen in Fig. 5(b), AMEE method produces the most similar endmember to ground-truth. As a general result for all tested methods, even though there was a 2:1 ratio in pixel area, no new endmembers appeared in the high-resolution images that were not seen in the lower resolution data, only purer spectra of known materials. This result was not surprising in light of the fact that the pixel size in low resolution imagery (2.4 meters) is large enough to identify pixels which are relatively pure, i.e. not mixed with surrounding material, in Dehesa ecosystems.

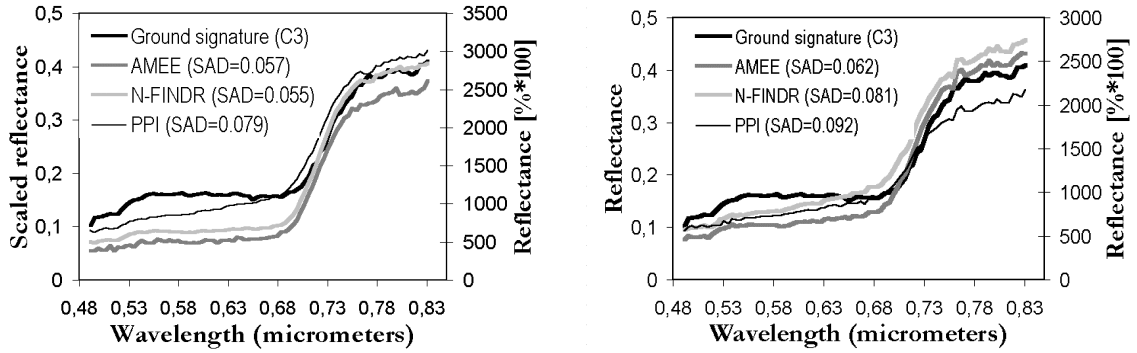

Figure 5. Cork-oak spectral endmembers derived by the three tested methods at two different resolutions: HRC3 (a) and LRC3 (b). The spectral angle distance between each endmember and a ground-truth spectral signature, collected at the test site, is shown for comparative purposes.

4.2 Experiment 2

In this experiment, we assume that the endmembers are relatively uniformly distributed among all pixels. With this assumption in mind, we derived abundance fractions in the low altitude data, i.e. HRC4, that can be directly compared with high-altitude, i.e. LRC4, abundance estimates by using available 2:1 ratio in pixel area. Conventional wisdom dictates that an endmember, filling a portion of a pixel, will become less detectable as the pixels are averaged, because its contribution to the total averaged spectrum will decrease. In order to test the above remark, we applied three different endmember extraction procedures (PPI, N-FINDR and AMEE) to HRC4 and LRC4 subscenes, using the same algorithm parameters considered in experiment 1 (see previous subsection). As a result, we can visualize the performance of the above endmember extraction methods, in the presence of different spatial resolutions, by plotting low-resolution-derived in contrast to high-resolution-derived abundances for the different constituents at each image pixel.

In Fig. 6, scatterplots of high-resolution versus low-resolution estimated abundance values, along with resulting correlation coefficients, are shown for each method and detected material (cork-oak trees, soil and pasture). Table 2 shows the root mean square error (RMSE) obtained when comparing abundance estimations at the two different resolutions. In general, we can observe in Fig. 6 that acceptable quantitative agreements between the low-resolution and high-resolution estimates are obtained in most cases. This fact seems to indicate that the low spatial resolution data (2.4 meter pixels) may be sufficient to accurately characterize Dehesa environments in terms of mixed pixel analysis. In addition, although table 2 shows that the three methods tested produce RMSE scores which are always below 10% error, it can be noticed that AMEE method [see Fig. 5(g-i)] produces lower RMSE scores than PPI [Fig. 5(a-c)] and N-FINDR [Fig. 5(d-e)]. This finding objectively confirms our insight: that the incorporation of spatial information in endmember selection improves mixed pixel classification accuracy by reducing algorithm sensitivity to low spatial resolution, as well as to noise and mixture complexity.

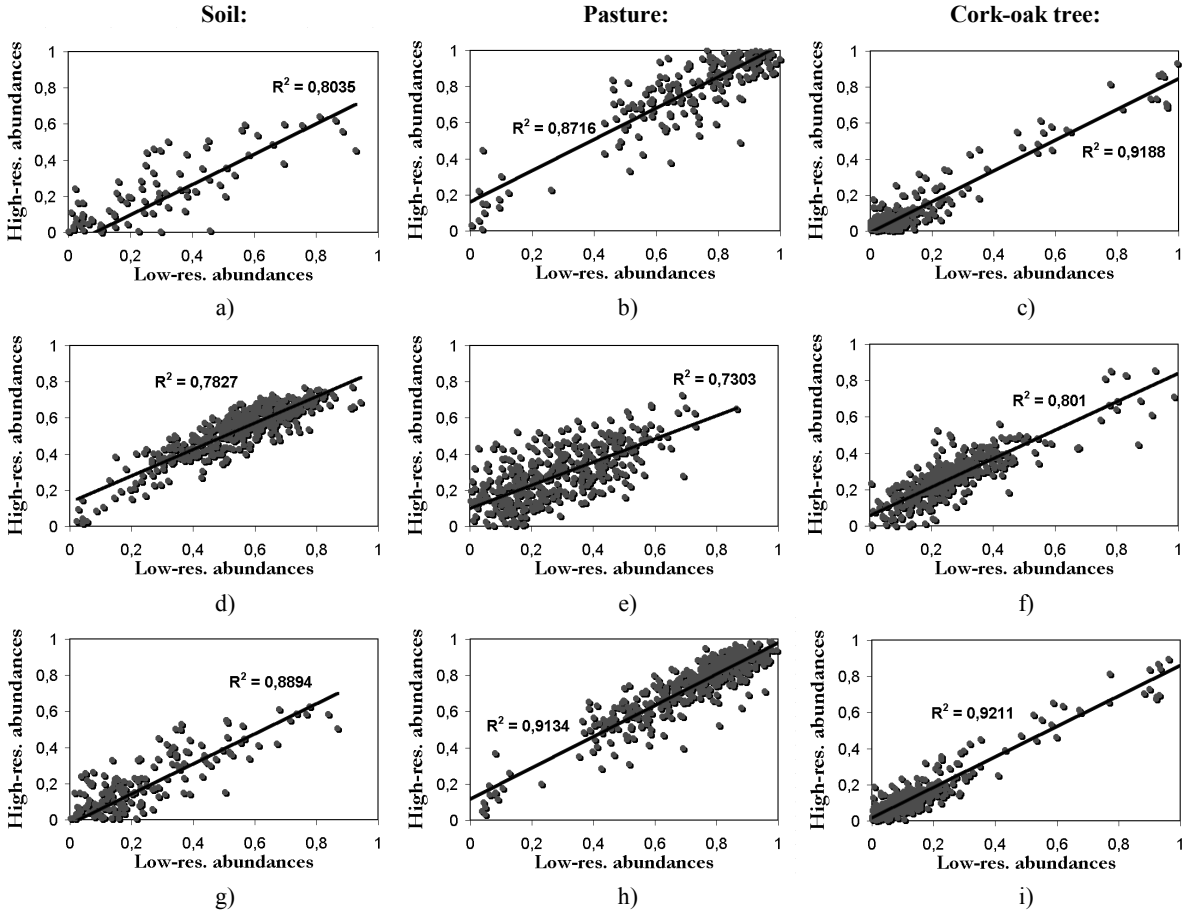

Figure 6. Scatterplots of low-resolution versus high-resolution abundances for soil, pasture and cork-oak tree, respectively, obtained after applying PPI (a–c), N-FINDR (d–f), and AMEE (g–i) methods to the pair of correspondent scenes HRC4, LRC4.

Table 2. RMSE error (%) obtained after comparing high-resolution estimated abundances to low-resolution estimated abundances using a pixel-by-pixel basis.

	PPI	N-FINDR	AMEE
Cork-oak	4.1	6.5	3.9
Soil	9.2	6.1	7.1
Pasture	8.2	9.3	6.2

5 CONCLUSIONS AND FUTURE WORK

In this paper, we have examined the influence of spatial resolution on the relevant task of extracting image endmembers for spectral mixture analysis of hyperspectral data. Results show that those methods that combine spatial and spectral information in the process of identifying endmembers produce results which are more robust to spatial resolution than those found with methods that use spectral information alone. One of the major questions that arise from this work is: to what extent spatial averaging of geophysical variables and distortion introduced by geometric registration techniques have an influence on abundance estimation errors obtained by using spectral mixture analysis techniques? The results obtained in this work reveal that the above phenomena are particularly important when dealing with mixed pixels, which are usually modeled by applying very accurate sub-pixel analysis techniques. In order to quantify the magnitude of the errors introduced by spatial averaging and geometric registration in sub-pixel analysis, further work is still needed. In particular, future research should be focused on analyzing the influence of the above-mentioned sources of error on non-linear spectral mixture analysis techniques,

which may be more appropriate than linear approaches in certain applications, especially those involving mapping of vegetation canopies.

ACKNOWLEDGEMENT

We would like to gratefully acknowledge DAIS and ROSIS teams at DLR for providing very high-quality hyperspectral data at different resolutions for our research, and also for their assistance and willingness to provide support in every single aspect of the hyperspectral data processing chain. In particular, we thank Andreas Müeller for leading the HySens project, which has provided an unprecedented opportunity for many European research groups to begin working with their own data. Also, we wish to thank Martin Habermeyer for his lead of the field spectroscopy team in Cáceres, and Rolf Richter for his supervision of the data pre-processing effort. We would also like to thank other scientists that have strongly contributed to the work presented in this paper, including Robert O. Green, who assisted us in the development of techniques for data analysis, and Michael E. Winter, who provided us with results and a demo version of his N-FINDR endmember extraction algorithm.

REFERENCES

[1] P.-F. HSIEH, L. C. LEE, N.-Y. CHEN, "Effect of spatial resolution on classification errors of pure/mixed pixels in remote sensing," *IEEE Transactions on Geoscience and Remote Sensing*, vol. 12, pp. 2657-2663, 2001.

[2] C.-I CHANG, *Hyperspectral imaging: spectral detection and classification*, Kluwer Academic Publishers, 2003.

[3] D. SCHLÄPFER, P. MEYER, AND K. I. ITTEN, "Parametric geocoding of AVIRIS data using a ground control point derived flighpath," *Summaries of the VIII JPL Airborne Earth Science Workshop*, Pasadena, CA, 1998.

[4] P. MARTINEZ, A. PLAZA, A. ATKINSON. "Generation of a Test Image to Validate the Performance of Endmember Extraction and Hyperspectral Unmixing Algorithms," *DLR/HySENS Users Meeting*, Oberpfaffenhofen, Germany, 2002.

[5] N. KESHAVA, J.F. MUSTARD, "Spectral unmixing," *IEEE Signal Processing Magazine*, vol. 19, pp. 44-57, 2002.

[6] J.M. CHEN, "Spatial Scaling of a Remotely Sensed Surface Parameter by Contexture". *Remote Sensing of Environment*, vol. 69, pp. 30-42, 1999.

[7] J. SETTLE, "On the relationship between spectral unmixing and subspace projection," *IEEE Transactions on Geoscience and Remote Sensing*, vol. 34, pp. 1045-1046, 1996.

[8] A. MÜELLER, A. HAUSOLD, P. STROBL, "HySens – DAIS / ROSIS Imaging Spectrometers at DLR," *Proc. VIII SPIE International Symposium on Remote Sensing*, Toulouse, France, 2001.

[9] F. J. PULIDO, M. DÍAZ, M., S. J. HIDALGO, "Size structure and regeneration of spanish holm oak quercus ilex forests and dehesas: Effects of agroforestry use on their long-term sustainability," *Forest Ecology and Management*, vol. 146, pp. 1-13, 2001.

[10] J. W. BOARDMAN, F. A. KRUSE, R. O. GREEN, "Mapping target signatures via partial unmixing of AVIRIS data," *Summaries of the VI JPL Airborne Earth Science Workshop*, Pasadena, CA, 1995.

[11] M. E. WINTER, "N-FINDR: An algorithm for fast autonomous spectral end-member determination in hyperspectral data," *Proc. SPIE Imaging Spectrometry V*, San Diego, CA, 1999.

[12] A. PLAZA, P. MARTINEZ, R. PEREZ, J. PLAZA, "Spatial/spectral endmember extraction by multidimensional morphological operations," *IEEE Transactions on Geoscience and Remote Sensing*, vol. 40, no. 9, pp. 2025-2041, 2002.

[13] A. PLAZA, *Proposal, validation and testing of a new morphological method for the analysis of hyperspectral data which combines spatial and spectral information*, Ph.D. dissertation (in Spanish), Computer Science Department, University of Extremadura, Spain, 2002.

[14] A. PLAZA, P. MARTINEZ, J.A. GUALTIERI, R.M. PEREZ, "Spatial/spectral identification of endmembers from AVIRIS data using mathematical morphology," *Summaries of the X JPL Airborne Earth Science Workshop*, Pasadena, CA, 2001.

[15] A. PLAZA, P. MARTINEZ, R. PEREZ, J. PLAZA, "A comparative analysis of endmember extraction algorithms using AVIRIS hyperspectral imagery," *Summaries of the XI JPL Airborne Earth Science Workshop*. Pasadena, CA, 2002.

[16] J. PLAZA, A. PLAZA, P. MARTINEZ, R.M. PEREZ, "H-COMP: A Tool for Quantitative and Comparative Analysis of Endmember Identification Algorithms," *IEEE International Geoscience and Remote Sensing Symposium (IGARSS)*, Toulouse, France, 2003.